Citation: Molecular Therapy — Methods & Clinical Development (2016) **3,** 16037; doi:10.1038/mtm.2016.37
Official journal of the American Society of Gene & Cell Therapy
www.nature.com/mtm

ARTICLE

Widespread AAV1- and AAV2-mediated transgene expression in the nonhuman primate brain: implications for Huntington's disease

Piotr Hadaczek[1], Lisa Stanek[2], Agnieszka Ciesielska[1], Vivek Sudhakar[1], Lluis Samaranch[1], Philip Pivirotto[1], John Bringas[1], Catherine O'Riordan[2], Bryan Mastis[2], Waldy San Sebastian[1], John Forsayeth[1], Seng H Cheng[2], Krystof S Bankiewicz[1] and Lamya S Shihabuddin[2]

Huntington's disease (HD) is caused by a toxic gain-of-function associated with the expression of the mutant huntingtin (htt) protein. Therefore, the use of RNA interference to inhibit Htt expression could represent a disease-modifying therapy. The potential of two recombinant adeno-associated viral vectors (AAV), AAV1 and AAV2, to transduce the cortico-striatal tissues that are predominantly affected in HD was explored. Green fluorescent protein was used as a reporter in each vector to show that both serotypes were broadly distributed in medium spiny neurons in the striatum and cortico-striatal neurons after infusion into the putamen and caudate nucleus of nonhuman primates (NHP), with AAV1-directed expression being slightly more robust than AAV2-driven expression. This study suggests that both serotypes are capable of targeting neurons that degenerate in HD, and it sets the stage for the advanced preclinical evaluation of an RNAi-based therapy for this disease.

Molecular Therapy — Methods & Clinical Development (2016) **3**, 16037; doi:10.1038/mtm.2016.37; published online 29 June 2016

INTRODUCTION

The ability of vectors derived from adeno-associated virus (AAV) to stably transduce a broad range of dividing and postmitotic cells with high efficiency makes AAV-based vectors attractive for development as central nervous system (CNS) gene therapies.[1] An important element of a successful gene therapy treatment is the choice of an appropriate AAV serotype. Although AAV2 is neurotropic, other serotypes (*e.g.*, AAV1, AAV5, AAV7, AAV8, AAV9, and AAVrh10) have a high affinity for neurons, astrocytes, and other non-neuronal cells.[2–9] Tropism is important not only for targeting specific cells in the brain but also for avoiding the transduction of cells that could trigger an immune response to a non-self protein.[10,11] The clinical failure of potentially effective molecular therapeutics is often due not to a lack of potency, but to shortcomings in the method by which they are delivered.

Huntington's disease (HD) is caused by a CAG repeat expansion mutation that encodes an elongated polyglutamine (polyQ) repeat in the mutant huntingtin protein (mHtt). HD is a particularly attractive target for DNA- and RNA-based therapies because it is an autosomal dominant disease. Recombinant AAV vectors provide an ideal delivery system for nucleic acid therapeutics as they can enable the permanent expression of huntingtin-lowering molecules in the brain. AAV-mediated gene therapies to deliver huntingtin-lowering strategies have shown great promise for HD, as indicated by the robust efficacy data presented in several preclinical studies.[12–16] To achieve maximal clinical efficacy in HD, delivery of a vector to both the striatum and cortex will likely be required. Postmortem analysis of HD patient brains revealed extensive medium spiny neuronal loss in the striatum in addition to the loss of pyramidal neurons in the cerebral cortex.[17,18] A recent report showed that genetically reducing m*HTT* expression in neuronal populations in both the striatum and the cortex of conditional transgenic mouse models of HD provides a significantly higher level of therapeutic efficacy than reducing m*HTT* in either of these regions of the brain alone.[19] This evidence suggests that delivering gene therapy agents to both striatal and cortical regions would be ideal to achieve maximal therapeutic efficacy. Demonstrating that the requirements for therapeutic efficacy can be translated from mice to larger animal species, whose anatomical characteristics are more reflective of those in human patients, is imperative.

The presence of the blood–brain barrier impedes vector transfer to the CNS after systemic delivery. Recent studies have demonstrated that the AAV9 serotype can cross the blood–brain barrier after systemic delivery. However, this led to predominantly astrocytic transduction.[20,21] Furthermore, although systemic delivery of AAV9-RNAi to N171-82Q mice significantly reduced *HTT* in multiple brain regions, it was not associated with motor improvements.[22] For almost two decades, the optimal conditions for direct brain delivery of viral vectors via convection-enhanced delivery (CED) have been extensively evaluated.[23–26] A new, reflux-free, stepped-design cannula that permits the use of CED with higher flow rates

The first two authors contributed equally to this work.

[1]Interventional Neuro Center, Department of Neurological Surgery, University of California San Francisco, San Francisco, California, USA; [2]Rare Disease Unit, Neuroscience, Sanofi-Genzyme, Framingham, MA, USA. Correspondence: LS Shihabuddin (Lamya.Shihabuddin@genzyme.com) Or KS Bankiewicz (Krystof.Bankiewicz@ucsf.edu)
Received 2 December 2015; accepted 13 April 2016

(>5 µl/minute) has been developed.[27] This study was designed to explore the potential use of AAV-mediated gene therapies to deliver Htt-lowering therapeutics to critical regions of the brain that are involved in HD. The goal was to evaluate specifically the potential use of AAV1 or AAV2 as a delivery vector because a majority of the preclinical studies have been conducted with AAV1, whereas most clinical studies to date for CNS applications have used AAV2 as a delivery vehicle. Multiple reports in the literature suggest the presence of differences in the cellular tropism and the capability of these vectors for retrograde and anterograde transport that depend on the serotype used and the delivery parameters.[28] However, the majority of these studies have not provided an appropriate characterization of the vector preparations used, which would better clarify the differences that have been reported regarding vector tropism and biodistribution. Thus, the use of the recombinant vectors AAV1-eGFP and AAV2-eGFP for *in vivo* gene delivery into the striatum of NHP brains via CED under MR-guidance was examined. Two different methods of vector production were used: triple transfection (TT) and a more scalable clinical manufacturing platform, producer cell line (PCL). A comprehensive analysis of the distribution, tropism, and efficacy of the resulting transduction was performed in the brains of 9 Rhesus macaques. Our results show robust AAV-mediated expression within the striatum and several cortical regions that are relevant to HD. The current data are promising and they suggest that the striatal CED delivery of AAV1 and AAV2 vectors results in transduction of brain areas that are critical for the treatment of HD. Furthermore, optimization of the delivery parameters for AAV1 or AAV2 may lead to global transgene delivery and may help in the design of new AAV-mediated gene delivery systems in future clinical trials for HD and other neurodegenerative diseases.

RESULTS

To better understand the potential usefulness of AAV1- or AAV2-mediated gene delivery for CNS diseases and to determine their specific cellular tropism within most of the affected brain regions relevant to HD, the expression of enhanced green fluorescent protein (eGFP) in the nonhuman primate brain was evaluated 4 weeks after injection of either AAV1-eGFP or AAV2-eGFP into the caudate and putamen. The dosing groups are summarized in Table 1. To date, the majority of preclinical studies have utilized vectors made by TT followed by purification with cesium chloride centrifugation or column chromatography. Thus, to evaluate the impact of vector production on biodistribution *in vivo*, two methods of vector production, TT and PCL, were compared. The vectors produced with either production platform were purified via the same proprietary column purification method. Thorough vector characterization was performed with a number of well-validated quality control assays and analytical tools. TaqMan PCR was used to determine vector concentration or particle titer[29] and a replication-based rAAV titration assay in a rep-cap-expressing HeLa cell line and end-point dilution PCR, was used to determine infectious titers.[29] Both TT and PCL generated AAV2-eGFP and AAV1-eGFP vectors, had infectious titers in agreement with AAV1 and AAV2 assay controls. Vectors generated by the PCL method were also assayed for residual adenovirus protein and infectious adenovirus by western blot analysis and replication PCR assay (E2A target), respectively. Both assays confirmed that vectors generated by PCL were substantially free of residual adenovirus. Analytical ultracentrifugation (AUC), was used to assess the ratio of full: empty capsids, as previously described.[30] All vectors were composed predominantly of full particles. Endotoxin levels were within levels deemed acceptable for animal studies as determined by LAL-Gel Clot Method and bioburden levels by membrane filtration. The purity of final vector lots were evaluated by sodium dodecyl sulfate–polyacrylamide gel electrophoresis and the proteins were visualized by SYPRO staining. VP1, VP2, and VP3 capsid protein bands were clearly resolved with no other impurities detected. More details about the vectors are summarized in Table 2.

Infusion performance

In all of the groups, which included AAV1-eGFP (TT), AAV2-eGFP (TT), AAV1-eGFP (PCL), and AAV2-eGFP (PCL), 90 µl of each vector was mixed with gadolinium contrast agent (2 mmol/l Prohance; Bracco Diagnostics, Monroe Township, NJ) and then infused into each striatum (60 µl into the putamen and 30 µl into the caudate nucleus). Magnetic resonance images (MRI) from each infusion confirmed that the positioning of each cannula was accurate and that the infusate covered the target area with occasional leakage to internal capsule. In addition, the ratio (Vd/Vi) between the volume of distribution (Vd) and the volume of infusion (Vi) was calculated for each delivery. Across all infusions, the Vd was approximately threefold larger (range 2.1–4.6) than the Vi (see Table 3 for summary and Supplementary Table S1 for details).

GFP transgene expression in the brain

After bilateral injection of either AAV1-eGFP or AAV2-eGFP (both TT and PCL) into the striatum of NHPs, robust expression of GFP was evident throughout both of the target structures (putamen and caudate nucleus) as well as their projection regions (the external and internal globus pallidus, GPe and GPi; substantia nigra, SN; subthalamic nucleus, and cortical regions in neuronal layers IV and V) (Figure 1). To evaluate the role of gadolinium as a marker of vector distribution in the striatum, we calculated the ratio of the area of GFP expression (from histological sections) to the area of gadolinium signal on corresponding MR scans. For monkeys infused with AAV1, this ratio was 1.21 ± 0.10, whereas it was 0.74 ± 0.04 for those infused with AAV2 (Figure 2). A ratio of 1.0 indicates a perfect match between GFP expression and MRI of vector distribution. This difference indicated that the AAV1 vectors distributed beyond the gadolinium signal and achieved better spread within the striatum (the targeted brain region) than the AAV2 vectors.

In addition to the ratios depicting vector dissemination capabilities, striatal coverage of GFP expression confirmed that AAV1 transduced larger areas (~19% more) of the striatum (putamen + caudate) than AAV2 (83.6 versus 70.1%; $P = 0.0002$ by unpaired two-tailed *t*-student test; see Table 3 for summary and Supplementary Table S1 for individual results). By projecting the extent of GFP expression onto the MRI scans of each monkey brain, we also calculated the percentage of GFP expression coverage in the cortex—a structure directly connected to the targeted striatum via axonal projections. (see Table 3 for summary and Supplementary Table S1 for further details). In all of the monkeys, we transduced, on average, 77.6% of the striatum, which resulted in substantial expression of GFP in the cortex (Figure 1). The extent of GFP expression in the cortex did not correlate with the AAV serotype used (AAV1 versus AAV2) (see Table 3 for summary of cortical coverage of GFP expression) or the method of vector production (TT versus PCL). Also, it seems that there was not always a clear correlation between broader distribution of the infusate within the infusion site (striatum) and the extent of transduction in the cortex. One NHP, MMU39956, (AAV1-eGFP (TT)) showed particularly robust GFP expression in cortical regions (layers IV and V) throughout the entire cortex (both frontal and

Table 1 Dosing groups

Group	*Production method*	*Vector*	*Vector concentration (vg/ml)*	*Vector dose per hemisphere (vg)*[a]	*Infectious titer (IU/ml)*
Cohort 1 (TT)					
AAV1-eGFP ($n = 3$)	TT	ssAAV2/1-CBA-eGFP	1.9×10^{12}	1.7×10^{11}	8.75×10^{9}
AAV2-eGFP ($n = 2$)		ssAAV2/2-CBA-eGFP	1.9×10^{12}	1.7×10^{11}	3.2×10^{11}
Cohort 2 (PCL)					
AAV1-eGFP ($n = 2$)	PCL	ssAAV2/1-CBA-eGFP	2.23×10^{12}	1.7×10^{11}	2.3×10^{9}
AAV2-eGFP ($n = 2$)		ssAAV2/2-CBA-eGFP	1.4×10^{12}	1.3×10^{11}	1.5×10^{11}

[a]vg, vector genome; TT, triple transfection; PCL, producer cell line.

Table 2 Characterization of the vectors used in the study

	AAV1-CBA-eGFP		*AAV2-CBA-eGFP*	
Assay/method[a]	*TT*	*PCL*	*TT*	*PCL*
Vector concentration TaqMan PCR (vg/ml)	1.9 e12	2.23 e12	1.9 e12	1.43 e12
Infectious titer assay (end point dilution/PCR) (IU/ml)	8.75 e9	2.3 e9	3.2 e11	1.5 e11
Full capsid (AUC) (% vector genome containing capsids)	70	78	60	69
Residual adenovirus protein (western)	NA	Undetectable	NA	Undetectable
Residual infectious adenovirus (limit assay/PCR) vg	NA	<10 IU/2.23 e11	NA	<10 IU/1.43 e11
Endotoxin (LAL-Gel Clot method) (EU/ml)	<0.3	<0.3	<0.3	4.8
BioBurden (membrane filtration) (CFU/0.2 ml)	0	0	0	0

AUC, area under curve; NA, not available; PCL, producer cell line; PCR, polymerase chain reaction; TT, triple transfection.
[a]*In vitro* assays do not reflect the performance/behavior of vectors *in vivo*.

Table 3 Infusion of AAV1-eGFP and AAV2-eGFP into the nonhuman primate brain and the extent of vector distribution within the brain 4 weeks after transduction

V_d/V_i[a]	*Gadolinium coverage*[b]	*Striatal coverage of GFP expression*[c]	*Cortical coverage of GFP expression*[d]
AAV1-eGFP			
2.79 ± 0.44	Putamen: 29.5 ± 10.9%; Caudate: 18.3 ± 5.2%	83.6 ± 7.8%	62.2 ± 19.1%
AAV2-eGFP			
3.29 ± 0.75	Putamen: 23.5 ± 9.3%; Caudate: 24.6 ± 8.0%	70.1 ± 10.2%	61.3 ± 14.8%

[a]Ratio of volume of distribution (Vd) to volume of infusion (Vi) was calculated (OsiriX Imaging software, v. 3.1) by dividing the volume of vector distribution within the injected brain parenchyma (based on the Gadolinium signal from MRI scans) by the volume of the injected vector. Values from left and right hemispheres were added to determine the average Vd/Vi for each animal. [b]Gadolinium coverage within targeted structures was calculated (OsiriX Imaging software, v. 3.1) by dividing Vd by the volume of Putamen (600 mm^3) or Caudate (500 mm^3). [c]Striatal GFP expression coverage was calculated from immunohistochemical analysis (IHC)-stained sections by dividing the area (mm^2) of GFP signal by the area of the targeted structure (caudate and putamen for each animal were calculated separately and expressed as percentage of GFP coverage). The average means for each group (AAV1-eGFP and AAV2-eGFP) are given in the table. For individual results from each animal, see Supplementary Table S1. The mean striatal coverage of GFP expression in animals injected with AAV1-eGFP was 19% higher than in animals injected with AAV2-eGFP group ($P = 0.0002$; unpaired two-tailed *t*-test). [d]Cortical GFP coverage was calculated by projecting GFP signal from matching IHC-stained sections onto corresponding MRI scans of each monkey (OsiriX Imaging Software version 3.1). No statistical difference was observed between animals injected with AAV1-eGFP and AAV2-eGFP.

occipital, see Figure 1a). Other animals showed variability in cortical expression associated with variations in both the extent and the localized anatomical regions transduced within the caudate and putamen. Because both precommissural and commissural regions of the striatum were targeted, more GFP was detected in the frontal and parietal cortical regions than in the occipital cortex.

Tropism and the efficiency of neuronal transduction

For both groups of NHPs transduced with AAV1-eGFP vectors (TT and PCL), examination of the morphology of GFP-positive cells suggested both neuronal and astrocytic transduction (Figure 3a,c–e). We confirmed this by double immunofluorescence staining with a combination of antibodies against GFP and NeuN (a neuronal

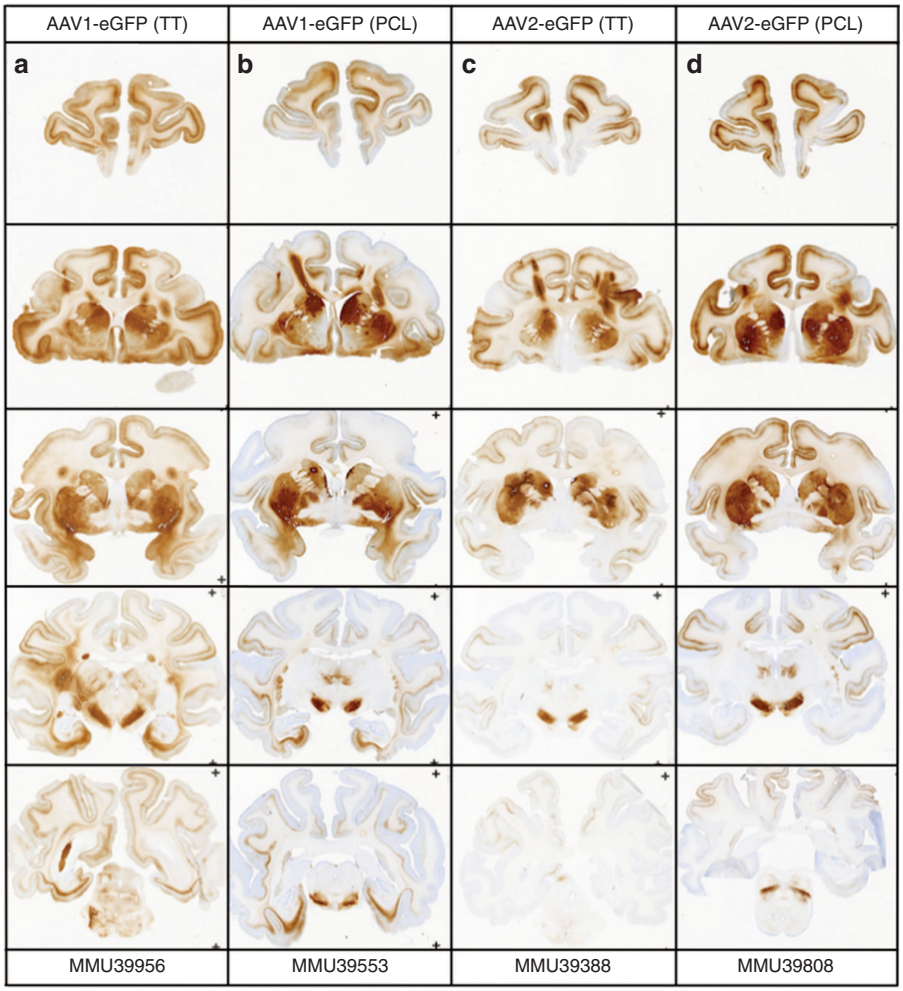

Figure 1 Distribution of GFP in the nonhuman primate brain infused with AAV1-eGFP and AAV2-eGFP. AAV1-eGFP and AAV2-eGFP vectors were infused bilaterally into the striatum of nine Rhesus macaques (see details in Materials and Methods). Four weeks after the surgery, brains were processed for immunohistochemistry (IHC) against GFP. Four columns show representative GFP-stained brain sections from four study groups infused with AAV1-eGFP (triple transfection (TT))—**column a**; AAV1-eGFP (producer cell line (PCL))—**column b**; AAV2-eGFP (TT)—**column c**; AAV2-eGFP (PCL)—**column d**. Representative sections show various coronal planes of the brain to demonstrate distribution of GFP expression throughout the entire brain from frontal cortex, striatum (infusion sites), midbrain, to occipital parts of the cortex. All groups show robust GFP expression in the sites of injection (putamen and caudate nucleus) as well as extensive transport to cortical regions and substantia nigra. Based on the IHC staining, the coverage of GFP expression in both target structure (striatum: putamen and caudate) and cortical regions were calculated for each monkey and are summarized in **Table 3**.

marker) or GFP and S-100 (an astrocytic marker) (Figure 4a–c). Animals administered AAV2-eGFP (both TT and PCL) exhibited predominantly neuronal transduction (Figure 3b,g,h). In addition, to further characterize the subtypes of transduced neurons, we used several neuronal markers and double immunofluorescence with GFP antibody. The main population of neurons transduced within the targeted structure, striatum, were medium spiny neurons indicated by costaining with anti-DARPP-32 antibody (GABAergic neurons, see Supplementary Figure S1a). As mentioned above, we detected GFP-positive neurons in distal brain structures receiving neuronal projections from the striatum. Here, GFP+ neurons were found in the substantia nigra pars compacta (SNpc), which contains dopaminergic neurons (colabeling with tyrosine hydroxylase, TH; see Supplementary Figure S1b) as well as in the substantia nigra pars reticulata (SNpr) composed of GABAergic neurons (costained with anti-γ-aminobutyric acid, GABA; see Supplementary Figure S1c). GFP-positive neurons within cortical regions turned out to be of glutamatergic origin indicated by costaining with anti-vGLUT-2 (vesicular glutamate transporter 2) antibody (Supplementary Figure S1d). GFP-positive cells of astrocytic lineage were also detected in the internal capsule (Figure 3f) and in cortical regions of white matter, where the infusion cannula tracks were visible. Based on the results of double immunofluorescence, we calculated the efficiency of neuronal transduction in the striatum and cortical regions (in the coronal plane of the infusion site) in all NHPs. Figure 5a summarizes our findings in the striatum. Individual calculations for each animal are shown in Supplementary Table S2. Striatal neuronal transduction in the regions of primary transduction, delineated by MRI, ranged from 50 to 65%. The highest efficiency of transduction was observed in NHPs infused with AAV1-eGFP (TT), with a mean of 64.2 ± 5.9%, and the lowest transduction was observed in the AAV2-eGFP (TT) group, with a mean of 46.6 ± 11.7% ($P = 0.0003$; unpaired two-tailed *t*-test; Figure 5a). Thus, it appears that AAV1 has an approximately 18% higher level of efficiency in transducing striatal neurons than AAV2. AAV1-eGFP produced by PCL resulted in a somewhat weaker ($P = 0.033$; unpaired two-tailed *t*-test) transduction of more neurons than AAV2-eGFP (59.5 ± 8.4 versus 50.1 ± 5.8%).

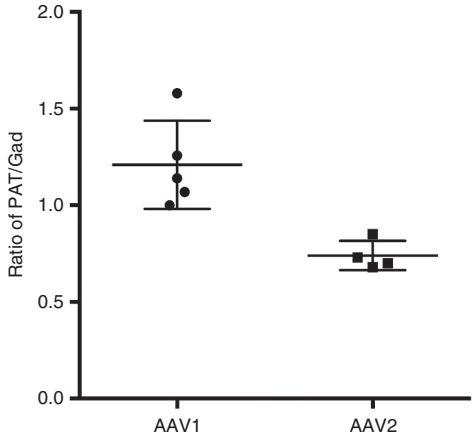

Figure 2 Ratios of primary areas of transduction (PAT) to vector distribution (Vd). Primary areas of GFP expression in the striatum were delineated on scans from the GFP-stained sections and their values were divided by values obtained from matching MRI scans with Gadolinium signal (see Materials and Methods). Ratios > 1.0 indicate that the extent of GFP expression exceeds the boundaries of Gadolinium signal after infusion. The results from monkeys infused with AAV vectors showed that AAV1 spreads better in the brain parenchyma than AAV2 (means + SD: 1.21 ± 0.1 versus 0.74 ± 0.04; $P = 0.007$ with two-tailed unpaired *t*-test).

The above calculations were derived from areas showing strong GFP transduction, as defined by MRI (primary area of transduction (PAT)). In addition, we calculated the efficiency of neuronal striatal transduction in regions outside the PAT to determine whether GFP-positive cells could also be detected beyond the clear boundary of strong GFP signal ("outside the primary area of transduction" (OPAT)), suggesting that perhaps all of the tested vectors had spread in a similar manner. The scheme by which these areas were chosen (random selection of five counting frames) is illustrated in Figure 5c. We observed a dramatic difference in the estimation of transduction efficiency in OPAT between the AAV1 and AAV2 serotypes (Figure 5b), with AAV1 transducing many more neurons than AAV2 (8.2 ± 3.9 versus 0.75 ± 0.26% ($P = 0.0001$) for the TT groups and 7.1 ± 3.5 versus 1.83 ± 0.9% ($P = 0.001$) for the PCL groups (both comparisons by unpaired two-tailed *t*-test). Individual calculations for each animal are shown in Supplementary Table S3. In addition, we calculated the efficiency of transduction in cortical regions that project to the striatum. Because the degree of cortical coverage varied among animals, we counted random cortical areas in sections with adjacent GFP-positive striatum. An evident discrepancy was observed among the animals (Supplementary Table S2) that showed no clear correlation between cortical efficiency of transduction and the serotype used. The mean cortical neuronal transduction efficiency for AAV1 was 13.6 ± 8.3%, whereas it was 13.4 ± 9.0% for AAV2 ($P = 0.97$).

As mentioned above, AAV1-eGFP transduced astrocytes (labeled with S-100) in addition to neurons. GFP-positive astrocytes were detected in the sites of primary transduction (striatum) and in cortical regions that project to the striatum. Examples of astrocytes transduced with AAV1-GFP are shown in Figure 4c. For the AAV2-eGFP vectors, only sporadic GFP+ astrocytes were detected surrounding the track of the infusion cannulae. Unfortunately, the number of transduced astrocytes could not be reliably quantitated in this study because the expression of foreign protein (GFP) causes astrogliosis (especially in the sites of vector injections); thus, documenting an increased number of astrocytes would be markedly biased. In addition, there were technical challenges in costaining

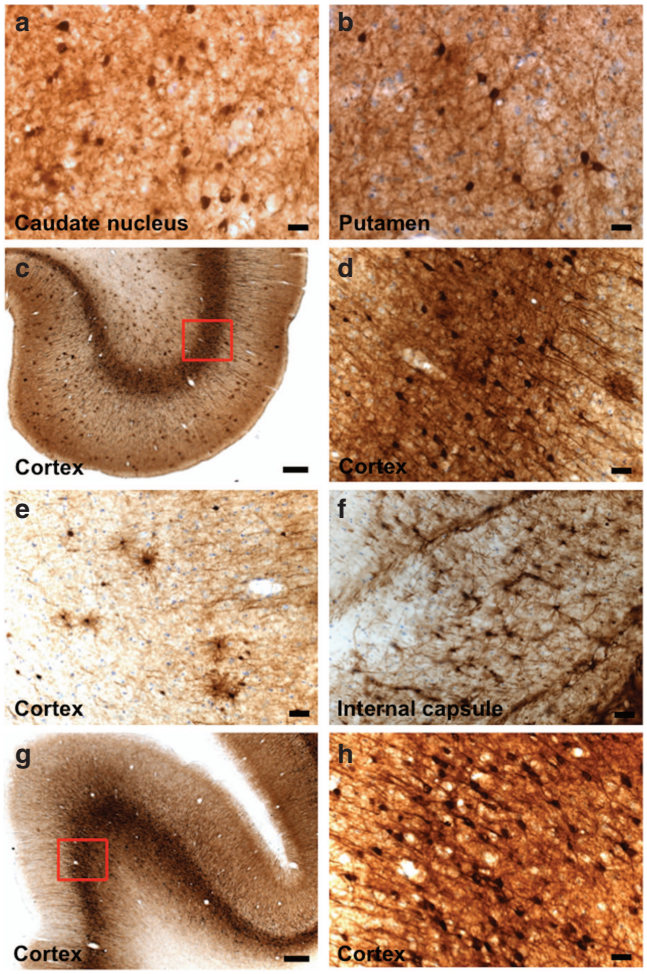

Figure 3 GFP expression in the nonhuman primate brain transduced with AAV1-eGFP and AAV2-eGFP. (**a**) High magnification (40×) of the target structure, caudate nucleus, transduced with AAV1-eGFP (TT) of monkey MMU39956. Dark-brown GFP+ neurons stained by 3,3'-diaminobenzidine (DAB) are visible against densely stained network of positive neuronal fibers. A robust signal was detected in all monkeys injected with AAV1-eGFP vector produced by both TT and PCL methods; size bar—50 µm. (**b**) High magnification (40×) of the target structure putamen transduced with AAV2-eGFP (TT) of monkey MMU39388. Dark-brown DAB signal shows expression of GFP in neurons and their densely stained network of fibers; size bar - 50 µm. **(c)** Fragment of prefrontal cortex of monkey MMU39956 (**column a in Figure 1**) demonstrating massive transport of vector AAV1-eGFP from the sites of injection (striatum) to cortical regions. Based on morphology of GFP+ cells, both neurons and astrocytes were detected in the cortex; size bar—500 µm. (**d**) Higher magnification (40×) of the frame from panel **c** showing numerous cortical neurons expressing GFP; size bar—50 µm. (**e**) High (20×) magnification of the cortex from monkey MMU39956 showing GFP+ cells of astrocytic morphology; size bar—100 µm. (**f**) High magnification (20×) of internal capsule of monkey MMU39388 showing GFP+ cells with astrocytic morphology; size bar—100 µm. (**g**) Fragment of prefrontal cortex of monkey MMU39388 (**column c in Figure 1**) demonstrating massive transport of vector AAV2-eGFP from the striatum (injection site) to cortical regions. The vast majority of GFP-positive cells had neuronal morphology (magnification 2.5×); size bar—500 µm. (**h**) Higher magnification (40×) of the frame from panel **g** showing numerous cortical neurons expressing GFP; size bar—50 µm.

of GFP-positive cells with astroglial markers. The intense GFP signal strongly competes with the S-100 antibody astrocyte marker. In areas of intense GFP signal the S-100 stain is almost completely suppressed. Additionally, the highly irregular shape of astrocytes

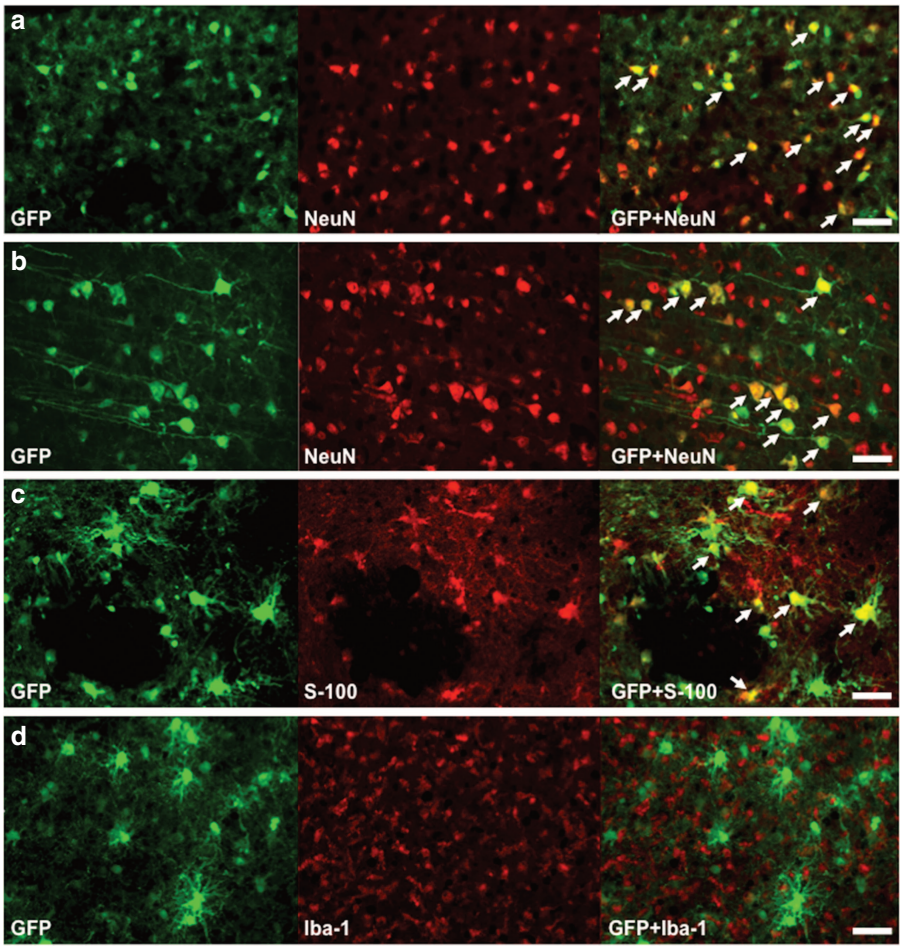

Figure 4 Cellular tropism of AAV1-eGFP and AAV2-eGFP injected into the monkey brain. Monkey brain sections were processed for double immunofluorescent staining against GFP and various cellular markers to determine cellular tropism of the injected vectors. (**a**) Section from caudate nucleus (target structure) from monkey MMU39956 stained with antibodies against GFP (green channel for DyLight 488 dye) and NeuN (neuronal marker) detected in red channel for DyLight 549 dye. Merged pictures (magnification 40×) from both channels show numerous neurons expressing GFP (white arrows), verifying neuronal tropism of AAV1-eGFP; size bar—50 µm. (**b**) The same staining was performed for a section from prefrontal cortex of monkey MMU39956 showing neuronal transduction (white arrows) in a distal brain structure receiving neuronal projections from the striatum and is evidence of retrograde transport of AAV1-eGFP; size bar—50 µm. (**c**) Section from caudate nucleus (target structure) from monkey MMU39956 stained with antibodies against GFP (green channel for DyLight 488 dye) and S-100 (astrocytic marker) detected in red channel for DyLight 549 dye. Merged pictures (magnification 40×) from both channels show numerous astrocytes expressing GFP (white arrows), verifying that AAV1-eGFP also transduces astrocytes; size bar—50 µm. (**d**) Section from caudate nucleus (target structure) from monkey MMU39819 stained with antibodies against GFP (green channel for DyLight 488 dye) and Iba-1 (marker for microglia) detected in red channel for DyLight 549 dye. The lack of costaining of both markers in merged picture (magnification 20×) indicates that AAV1 does not transduce microglia and this was also the case for AAV2 (data not shown; size bar—50 µm).

and presence of numerous processes makes reliable quantification of double-stained cells extremely difficult. Morphologically, there appeared to be more GFP-positive astrocytes in monkeys transduced with AAV1-eGFP than in those transduced with AAV2-eGFP.

To determine whether our vectors transduced other antigen-presenting cells in the brain, we costained representative brain sections from all monkeys with antibodies against GFP and the microglial marker, Iba-1. No animals showed double-labeled cells (Figure 4d). Moreover, staining against Olig-2, a marker for oligodendrocytes showed that only a few cells were positive for both GFP and Olig-2. Those sparse cells were detected mainly in the vicinity of the cannula tracks (data not shown).

Although this study was not primarily designed to assess the safety of AAV1- and AAV2-mediated transduction in NHP brains, we stained brain sections with hematoxylin-eosin (H&E) to determine whether these vectors triggered neuroinflammation. Sections were examined primarily for the presence of perivascular cuffing, indicative of the accumulation of lymphocytes or plasma cells in a dense mass around blood vessels. In two (MMU39956 and MMU39819) of the nine monkeys, varying degrees of infiltrates were detected in the primary areas of transduction (Supplementary Figures S2a,b) after AAV1-GFP administration. The remaining 7 NHP showed few signs of inflammation and no other vector/transgene-related histological findings were observed.

DISCUSSION

Paramount to the clinical success of an AAV-mediated strategy to lower huntingtin for the treatment of HD is the need to target neurons in disease-affected brain regions. Optimal therapy requires efficient cellular targeting within specific areas of the brain, especially in neurodegenerative diseases like HD, where the therapeutic gene acts in a cell-autonomous manner.[31] A number of factors make AAV a preferred gene delivery vehicle for CNS-focused clinical trials.[32] The current study demonstrates unequivocally for the first time,

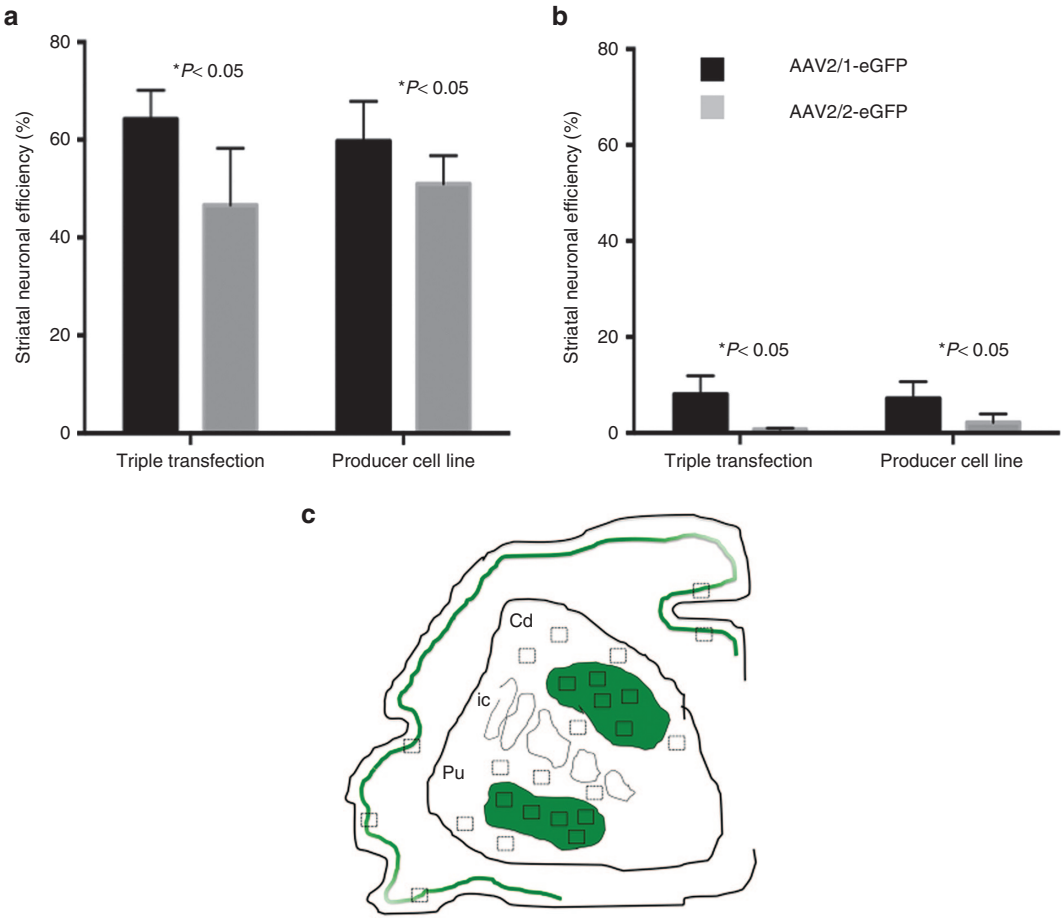

Figure 5 Efficiency of neuronal transduction in the striatum of nonhuman primate injected with AAV1-eGFP and AAV2-eGFP. Double immunofluorescent staining against GFP and neuronal marker, NeuN, of monkey brain sections was performed to calculate the efficiency of neuronal transduction within the striatum (target structure) and cortical regions. For the striatum, the efficiency of transduction was calculated in the primary area of GFP transduction (PAT) where signal was robust with densely distributed GFP+ neurons (**a**). Neurons were also detected in regions outside the primary areas of GFP transduction (OPAT, **b**). Scheme for the technique of counting GFP+ neurons in PAT (green color) and OPAT (outside green color) is shown in (**c**). Details on the counting methods are described in Materials and Methods. Data from individual counting for each monkey and brain structure are shown in Supplementary Table S2 (PAT) and and Supplementary Table S3 (OPAT). Cd, Caudate; ic, internal capsule; Pu, putamen.

that local striatal delivery of AAV1 or AAV2 can lead to robust global viral transduction and expression in brain areas that are central to HD pathology and potentially other neurodegenerative diseases.

A recent study showed that AAV1-mediated expression of a siRNA that targeted mutant human *HTT* led to a significant reduction in striatal levels of *HTT m*RNA and Htt protein in the YAC128 mouse model of HD and was associated with phenotypic improvements,[16] in agreement with previous preclinical studies.[12–15] Studies demonstrating similar efficacy in larger animal models of HD have not been realized because such models either exhibit no behavioral deficits or are more severe and have not been sufficiently characterized.[33] Efforts have, therefore, focused on demonstrating effective CNS delivery of surrogate AAV vectors that encode reporter genes to target CNS regions relevant to HD pathology. Selective neuronal loss in HD begins in the medial caudate and the posterior putamen. Hence, these structures were the primary targets of the present study. Some neuropathology was observed in cortical layers 3, 5, and 6, and in some cases, more global degeneration was observed.[34,35]

The current study is a comprehensive comparison of two AAV serotypes, AAV1 and AAV2, manufactured by two different methods (TT and PCL), infused into nonhuman primate (NHP) brains. Immunohistochemical analysis of NHP brains revealed significant transduction of the targeted structures (putamen and caudate nucleus) by both of the serotypes used, regardless of the method of production. However, AAV1 performed significantly better than AAV2 with regard to the extent of transduction that was achieved. By calculating the volume of GFP expression (Ve) in each animal and dividing it by the volume of infusion (Vi) in each case, the mean ratio for each group of animals (1.21 ± 0.1 for AAV1 and 0.74 ± 0.04 for AAV2) showed that AAV1-mediated expression was approximately 60% greater than AAV2-mediated expression for a given Vi. This result is in agreement with the results of a recent study,[36] wherein the authors used a different technique to measure expression in a different target structure (monkey cortex). However, the differential values were identical (1.2 ± 0.2 for AAV1 and 0.7 ± 0.2 for AAV2), confirming that AAV1 resulted in better tissue distribution in the brain than AAV2. Other investigators have also observed greater AAV1 spread within the striatum of NHPs[37] and smaller animals.[28,38] In addition to the ratios depicting vector dissemination, striatal coverage of GFP expression confirmed that AAV1 transduced larger areas (~19% more) of the striatum (putamen + caudate) than AAV2. As previously demonstrated, widespread axonal transport of the infused vectors from their primary areas of transduction (PAT) to other brain regions that are directly or indirectly connected with the

striatum[2,39] was clearly observed. For both vectors, transport to the internal and external globus pallidus (GPi and GPe) was observed as well as to the substantia nigra pars reticulata (SNpr) and compacta (SNpc). For AAV2-eGFP, transport was also observed to the subthalamic nucleus. Variable GFP signal in thalamic nuclei that project directly to the striatum was also observed.

One of the most intriguing findings was the extent of GFP expression seen in distal cortical regions. Previously, it was shown that viral delivery to axon terminal fields in the hippocampus and striatum resulted in viral internalization, retrograde transport, and transgene expression in specific projection neurons in the entorhinal cortex and substantia nigra.[40,41] Others have reported that AAV transport to the cortex occurs mainly through thalamocortical projections when AAV2 was infused directly into the thalamus itself.[42] In this study, the extent of thalamic expression varied considerably between NHPs and was likely due to axonal projections from the striatum; thus, the robust cortical transduction was likely the result of retrograde transport via cortico-striatal neurons that projected into the site of infusion (striatum). Retrograde transport of AAV1 has been reported previously,[43,44] but this is the first demonstration of such robust and extensive transport to cortical regions in the NHP brain after striatal transduction. A previous study of AAV1-hrGFP in NHPs did not detect any GFP+ cells in the cortex after putaminal infusion[2] with comparable doses (2.3×10^{11} vg versus 1.7×10^{11} vg in the current study) and delivery methods. It is important to note that the composition and source of those vectors, *i.e.*, its promoter, transgene (humanized GFP from *Renilla reniformis*) and the method of purification were different from those used in the present study. These differences in vector characteristics, quality, purification methods and the robust delivery method used in this study should not be underestimated and might explain the discrepancies reported in the AAV literature. Similarly, in our previous studies with AAV2 we have never observed cortical expression after administration of AAV2-AADC into the monkey striatum.[45,46] Although the total dose of the AAV2-AADC used in our 8-year survival study was > 50% higher (3.6×10^{11} vg) than in the current experiments (1.7×10^{11} vg for AAV2-eGFP produced by TT and 1.3×10^{11} produced by PCL), the striatal neuronal efficiency of transduction was eightfold smaller (6.1 ± 0.5% versus nearly 50% in the current study in the AAV2). This discrepancy is further reflected in recent neuropathological data showing cortical expression of neurturin after putaminal administration of AAV2-NRTN in parkinsonian patients.[31] Both those vectors were AAV2, but they differed in vector cassettes, production methods, and purification.

In the current study, the infectious titers for serotypes 2 (both for PCL and TT) are significantly higher (more than 10-fold) than for AAV1 and yet the *in vivo* performance is better for the AAV1 serotype. The difference in infectivity values are a reflection of tropism differences between AAV1 and AAV2 for the HeLa rep/cap cell line, thus *in vitro* infectivity values cannot be used to compare *in vivo* potency between serotypes. The infectivity of AAV1 made by PCL is similar to that made by TT, the same holds for AAV2. With respect to the percentage of full capsids (Table 2), the differences between the AAV preparations are not significant. Importantly, we dosed animals based on genome containing particles (measured by PCR) so all doses were equivalent.

Within the primary transduction area, AAV1 transduced more neurons than AAV2 (64.2 ± 5.9 versus 46.6 ± 11.7%). However, this difference was not reflected in the cortex. Better transduction by AAV1 in the primary infusion area could be due to more efficient internalization of virions because some studies have found that AAV5- or AAV1-transduced cells contain more virions than AAV2-transduced cells.[47,48] Different cellular primary receptors, such as high-affinity heparan sulfate proteoglycan (HSPG) for AAV2[49] and sialic acid for AAV1,[50] are required for viral entry and likely play a role here. Their affinities and abundance within the brain parenchyma may contribute to vector dissemination patterns. Different primary receptors and coreceptors were also responsible for the differences in cellular tropism observed in this study. AAV1 transduced both neurons and astrocytes, as reported previously by multiple investigators.[2,28,51]

The presence of GFP in the cortex with relatively limited striatal transduction is remarkable and suggests a high degree of convergence in the organization of cortico-striatal projections.[52] This may explain why even quite focal transduction of the striatum can result in transduction of broad areas of the cortex. Many comprehensive studies have mapped the organization of the cortico-striatal projection system and, although there is some degree of overlap in their terminal fields, each cortico-striatal fiber terminates in a highly arborized manner in the striatum.[52–55] This may explain the differences in GFP cortical coverage between individual monkeys. Although the putamen and caudate were targeted in each monkey, the primary pattern of GFP transduction was not identical between subjects (more ventral versus dorsal or more medial versus lateral), which was likely responsible for the patterns of retrograde transport to different regions of the cortex. Future studies to optimize and maximize the coverage of the transduced brain regions are warranted for preclinical development.

In addition to retrograde and anterograde transport, the observed widespread pattern of GFP expression maybe due to several modes of vector transport in the NHP brain. Although speculative, the transduction patterns noted in the distal cortical regions, such as the prefrontal and occipital lobes, suggest that the distribution was aided by virions tracking along the surface of white matter tracts. Another potential mechanism of distribution is movement of the viral vector through the Virchow-Robin space, a perivascular compartment that serves as a pipeline for interstitial fluid movement through the CNS.[56]

Safety in gene therapy clinical trials is of utmost importance. Previously, it was shown that AAV serotypes are capable of transducing antigen-presenting cells in the brain, which triggers an immune response if the transgene is of foreign origin, such as GFP.[2,10,57] When the gene encodes a self-recognized protein, no cell-mediated immune response is observed.[11] In the current study, none of the vectors transduced microglia, which are important immune effector cells in the CNS. In two primates, H&E staining revealed the presence of more pronounced perivascular infiltrates in the primary areas of transduction as well as a few activated astrocytes (hypertrophy of cellular processes, data not shown), as has been previously observed.[2,11] This type of transduction seemed to be correlated primarily with the presence of the foreign eGFP gene and with vector tropism. It is worth noting that no such activation or perivascular infiltration was detected beyond the PAT or in distal brain structures to which the vectors were transported (GP, subthalamic nucleus, SN, cortex).

This study comprehensively compared two serotypes of AAV (AAV1 and AAV2) and two methods of production (TT versus PCL) by their ability to transduce NHP brains in an exploratory study aimed at developing a treatment for HD. Because of differences in their dissemination properties, AAV1 transduced larger areas of the striatum with a higher efficiency of neuronal transduction. Furthermore, the data suggest that, even with only partial coverage of the putamen and caudate nucleus, large areas of the cortex can be transduced by retrograde transport of AAV from the primary infusion site. The

major lesson from the current study is that in order to generate consistent patterns of transgene distribution within the projected brain areas, (cortical regions), complete or nearly complete transduction of the targeted structures (striatum) should be achieved. This should certainly be further optimized and resolved before next clinical trials. The direct delivery of AAV vectors into the brain by CED has been under development for many years,[2,4,24,25,39,46,58,59] and clinical implementation of MR-guided CED of AAV has been achieved in two current clinical trials in Parkinson's disease (PD) (ClinicalTrials.gov: NCT01973543 and NCT01621581). Because striatal targets in PD and HD are similar, based on previous experiences with AAV2 delivery in PD, one can envisage striatal coverage that exceeds the range of the striatal transduction that has been achieved in this study by increasing the Vi, which in turn may result in more uniform and complete cortical expression. Thus, optimized targeted delivery of AAV to the striatum may be a viable approach for treating HD with gene transfer of a siRNA targeting *HTT*.

In conclusion, this is a pivotal study demonstrating that targeted delivery of AAV1 or AAV2 to the striatum results in robust and global transduction of the striatum as well as many cortical regions via axonal transport. These results far exceed the AAV1 and AAV2 transduction patterns previously reported in the literature, suggesting that differences in vector construct (sequence and promoter), methods of production, purification, and the analytical assays used to assess vector attributes (full genome particles, purity) may highly impact cellular tropism and capability of axonal transport. When aiming to advance gene therapy towards clinical applications, a clear characterization of vector attributes and an understanding of the delivery parameters that impact targeting need to be carefully evaluated in NHP studies. Our findings underscore the unrealized potential of AAV1 and AAV2 vectors to transduce multiple brain regions following localized infusions. The results validate that striatal delivery may be sufficient for the delivery of nucleic acid-based therapeutics to areas of the human brain relevant to HD and are highly supportive of continued translational research to advance this paradigm toward clinical testing.

MATERIALS AND METHODS

Animals

Nine adult male Rhesus macaques (*Macaca mulatta*; 8.9–11.9 kg) were included in this study. Animals received bilateral infusions, into caudate nucleus and putamen, of either AAV1-eGFP or AAV2-eGFP vectors that were obtained using two different production methods: TT or PCL. Vector concentrations and doses are described in Table 1. Animals were tested for the presence of anti-AAV1 and anti-AAV2 neutralizing antibodies, as previously described, and were considered seronegative if they presented antibody titers of < 1:32. Survival time was 1 month after AAV delivery for all of the animals. Experiments were performed according to the National Institutes of Health guidelines, and the protocols in this study were approved by the Institutional Animal Care and Use Committee at the University of California San Francisco.

In-life observations

Detailed cage-side observations of animal health, appearance, appetite and neurological symptoms were performed on a daily basis for a period of 5 days after dosing and weekly thereafter until the conclusion of the study. Body weight assessments were performed before intracranial dosing, at the time of blood collection procedures, and at necropsy. Whole blood, blood serum and cerebrospinal fluid were collected for hematology, serum chemistry, AAV1 and AAV2 capsid antibody assay, and eGFP mRNA level analysis.

Production of AAV vectors

AAV vectors were produced via either transient transfection[60] or the PCL method as previously described.[61,62] Briefly, to produce AAV vectors by the transient transfection method, HEK293 cells were transfected with polyethyleneimine and a 1:1:1 ratio of three plasmids (inverted terminal repeats (ITR) vector, AAV2rep/cap2 or AAV2rep/cap1 and pAd helper plasmid). The inverted terminal repeats vector plasmid encoded the cDNA for EGFP, downstream of the cytomegalovirus enhancer/chicken β-actin—hybrid promoter CBA. The pAd helper that was used was pHelper (Stratagene/Agilent Technologies, Santa Clara, CA). The generation of AAV vectors with the PCL method was performed as previously described.[61,62] Briefly, a HeLa-based PCL was created by transfection of HeLaS3 cells, (ATCC CCL-2.2) with a single plasmid containing the following elements: AAV2 rep genes and the cap gene of either serotype 1 or 2, the vector genome flanked by AAV2 inverted terminal repeats (ITRs), and a puromycin resistance gene. The vector genome harbored the cDNA for EGFP downstream of the cytomegalovirus enhancer / chicken beta actin hybrid promoter, CBA. Transfected cells were grown in the presence of puromycin to isolate stable integrants. Product-specific cell lines were expanded in a bioreactor and infected with wild-type adenovirus to initiate AAV production. Purification of AAV from both production platforms was performed as previously described.[63] The resulting titers of all AAV1-eGFP and AAV2-eGFP vectors are shown in Table 1. All vectors were suspended in a phosphate-buffered saline (pH 7.4) supplemented with 0.001% Poloxamer 188 (Lutrol F68). Vectors were characterized using a number of quality control assays (Table 2). Both TT and PCL generated AAV2-eGFP and AAV1-eGFP vectors, had infectious titers in agreement with AAV1 and AAV2 assay controls. The calculated particle: iu ratios for AAV1 eGFP, both TT and PCL produce, were consistent with typical values measured for AAV1 vectors, *i.e.*, ≤ 1,000:1,[64] while the particle:iu ratios for both AAV2-eGFP vectors were in agreement with previously reported rAAV2 particle:Iu ratios, *i.e.*, < 10:1.[29] AAV2 is more efficient at transducing HeLa cells, and this is reflected in the lower particle: iu ratio for AAV2-eGFP vectors produced either by TT or by PCL.

Vector infusion

All animals received a bilateral infusion of AAV vector into the caudate nucleus and putamen by means of MRI-guided CED.[23–25] Briefly, animals were sedated and then positioned in a stereotactic system with MR-compatible, skull-mounted, temporary cannula guides placed over each hemisphere. After a T1-weighted planning scan (Siemens 3.0 T Trio MR unit) to set the trajectory, a ceramic custom-designed fused silica reflux-resistant cannula with a 3-mm stepped tip was used for the infusion. Each animal received up to three infusions per hemisphere to target the caudate and the putamen (precommissural and postcommissural) regions. To visualize the infusate distribution during MRI, Prohance (2 mmol/l chelated Gadolinium) was added to the virus. Thirty microliters (30 µl) of AAV was infused into the caudate, and 60 µl was infused into the putamen (*i.e.*, 90 µl per hemisphere). The infusion rate was ramped up to a maximum of 5 µl/minute. Serial MRIs were acquired to monitor the infusate distribution within each target site and to provide real-time feedback to the surgical team.

The first cohort of animals received 1.7×10^{11} vg of AAV1-eGFP (TT) ($n = 3$) or AAV2-eGFP (TT) ($n = 2$) per hemisphere. The second cohort of animals received 1.7×10^{11} vg of AAV1-eGFP (PCL) ($n = 2$), or 1.3×10^{11} vg of AAV2-eGFP (PCL) ($n = 2$) per hemisphere. AAV2-eGFP (PCL) vector titers were slightly lower (1.4×10^{12} vg/ml), thus the total dose delivered per monkey of AAV2-eGFP (PCL) was slightly lower than that of AAV1-eGFP (TT), AAV2-eGFP (TT), and AAV2-eGFP (PCL). Immediately after the parenchymal dosing procedure, animals were monitored during recovery from anesthesia and then returned to their home cages.

MR imaging data analysis

Semi-quantitative analyses (Digital MRIs Vd/Vi). Distribution volume (Vd) analysis was performed using OsiriX Imaging Software version 3.1 (The OsiriX Foundation, Geneva, Switzerland). Infusion sites, cannula tracks and the cannula tip were identified on T1-weighted MR images in the coronal plane. Regions-of-interest were delineated to outline T1 gadolinium signals and the target sites (*i.e.*, the putamen and caudate nucleus). Three-dimensional volumetric reconstructions of the image series and regions-of-interest were analyzed to estimate the volume of distribution (Vd) of the infusions and the ratio to the volume of infusate (Vi).

Histological analysis of transgene expression. To assess transgene expression, brain sections were processed for immunohistochemical analysis. Animals were deeply anesthetized with sodium pentobarbital (25 mg/kg i.v.) and euthanized 4 weeks after administration of the vectors. The brains were removed and sectioned coronally into 6-mm blocks. The blocks were post-fixed in buffered paraformaldehyde (4%) for 24 hours, washed briefly in PBS

and immersed in 30% sucrose/phosphate-buffered saline (PBS) solution for cryopreservation. The formalin-fixed brain blocks were cut into 40-µm coronal sections with a cryostat. Free-floating sections spanning the entire brain were collected and stored in antifreeze solution for further analysis.

Immunohistochemistry

GFP staining by 3,3′-diaminobenzidine. Sections (three per each 6-mm block, with a separation of 2 mm) were washed three times in PBST for 5 minutes each time and then treated with 1% H_2O_2 for 20 minutes. Sections were incubated in Sniper blocking solution (http://biocare.net/product/background-sniper/) for 30 minutes at room temperature and then incubated overnight with the primary anti-GFP antibody (https://www.lifetechnologies.com/) diluted 1:1,000 in Da Vinci Green Diluent (http://biocare.net/). After three rinses in PBS containing 0.1% Tween-20 (PBST) for 5 minutes each time, sections were incubated in Mach 2 horseradish peroxidase (HRP) polymer (http://biocare.net/) for 1 hour and then washed three times before colorimetric development with 3,3′-diaminobenzidine. Immunostained sections were counterstained with cresyl violet, and mounted on slides and sealed with Cytoseal (http://www.thermoscientific.com/).

Calculation of coverage of GFP expression in the NHP brain. GFP staining from matching immunohistochemical analysis-stained serial sections was projected onto corresponding MRI scans from each NHP brain (T1-weighted MR images in the coronal plane). OsiriX Imaging Software version 3.1 (The OsiriX Foundation, Geneva, Switzerland) was used to determine the distribution/coverage of GFP expression. In addition, to calculate the striatal coverage of GFP expression, the ImageJ 1.44o software (NIH) was employed. The GFP coverage was calculated from immunohistochemically stained sections by dividing the area (mm^2) of GFP signal by the area of the targeted structure (caudate and putamen for each animal were calculated separately and expressed as percentage of GFP coverage).

Double-immunofluorescence for vector tropism and the efficiency of neuronal transduction. For double fluorescence immunostaining of different cellular markers (NeuN, S-100, Iba1, DARPP-32, TH, GABA, VGLUT2, and Olig-2) with GFP, a combination of primary antibodies was applied to sections as a cocktail of primary antibodies and overnight incubation at room temperature in PBST with 20% horse serum. The primary antibodies used were as follows: anti-GFP antibody (1:500, as above), anti-NeuN (1:500, http://www.emdmillipore.com/); anti-S-100 (1:300, http://biocare.net/), anti-Iba1 (1:500, http://biocare.net/), anti-DARPP-32 (1:500, http://www.scbt.com/), anti-TH (1:500, http://www.emdmillipore.com), anti-gamma-aminobutyric acid (GABA) (1:500, http://www.sigmaaldrich.com/), anti-VGLUT2 (1:200, https://www.emdmillipore.com) and anti-Olig2 (1:50, http://www.emdmillipore.com/). After three washes in PBST, primary antibodies were visualized by incubating the slides in the dark for 2 hours with the appropriate secondary fluorochrome-conjugated antibodies: goat anti-mouse DyLight 549 and goat anti-rabbit DyLight 488 (www.biocare.net/). All secondary antibodies were diluted 1:1,000 in Fluorescence Antibody Diluent (http://biocare.net/). In addition, to quench autofluorescence, sections were incubated in 0.1% Sudan Black solution (70% ethanol). After final washes in PBS, sections were cover-slipped with Vectashield Hard Set Mounting Medium for Fluorescence (www.vectorlabs.com/). Control sections were processed without primary antibodies, and no significant immunostaining was observed under these conditions.

A Zeiss Axioskop fluorescence microscope (www.zeiss.com/) equipped with a CCD color video camera and an image analysis system (AxioVision Software, www.zeiss.com/) was used to determine the presence of double-labeled cells (positive in both the red and green channels). Photomicrographs of double-labeled sections were obtained by merging images from two separate channels (red and green; colocalization appears as yellow) without altering the position of the sections or the focus (objective ×20). For GFP/NeuN double labeling, three sections from each animal at approximately 4-mm intervals were selected from the sites of vector infusion. To evaluate the efficiency of neuronal transduction by the AAV1-eGFP or AAV2-eGFP vectors within the targeted brain areas (the caudate and putamen), five counting frames (700×550 µm) were randomly placed in the GFP+ area. The primary area of transduction (PAT) was defined as the GFP-positive area ("cloud") that covered more than 40% of the targeted structure. Similarly, to evaluate the efficiency of neuronal transduction, in the area outside the PAT (OPAT), 5 counting frames (700×550 µm) from each section were chosen beyond the clear margins of the GFP-positive "cloud" in the targeted structures (the caudate and putamen) or in the cortex (Figure 5c). To determine the proportion of GFP/NeuN-positive cells, each counting frame was counted twice, first in the red channel to determine the number of NeuN+ cells and then in a combined red and green channel to determine the number of costained cells (GFP+ and NeuN+). At least 1,500 NeuN+ cells were counted for each of the three chosen sections (five counting frames per section). Finally, the percentage of GFP+/NeuN+ to total NeuN+ cells was determined. All of the calculations for the striatum were made by adding the results obtained from the analysis of both hemispheres in each animal and by combining the values from the putamen and caudate nucleus because the mean transduction efficiencies were identical in both of these structures in each animal.

CONFLICT OF INTEREST

Lisa Stanek, Catherine O'Riordan, Seng H. Cheng, and Lamya Shihabuddin are employees and shareholders at Sanofi Genzyme.

ACKNOWLEDGMENTS

This work was supported by Genzyme. The authors thank Jennifer Sullivan (Gene Therapy), Elton Kong, (Gene Therapy), Shelly Nass (Gene Therapy), Denise Woodcock (Gene Therapy), Maryellen Mattingly (Gene Therapy), Brenda Burnham (Gene Therapy), Rena Baek (Pharmacology and Toxicology), and the Gene Therapy Development group from Sanofi-Genzyme for their technical assistance and support of these studies. Richard Sidman (Professor of Neuropathology) from the Harvard Medical School for assistance in analysis of slides and critical reading of the manuscript.

REFERENCES

1. Peel, AL and Klein, RL (2000). Adeno-associated virus vectors: activity and applications in the CNS. *J Neurosci Methods* **98**: 95–104.
2. Hadaczek, P, Forsayeth, J, Mirek, H, Munson, K, Bringas, J, Pivirotto, P *et al.* (2009). Transduction of nonhuman primate brain with adeno-associated virus serotype 1: vector trafficking and immune response. *Hum Gene Ther* **20**: 225–237.
3. Davidson, BL, Stein, CS, Heth, JA, Martins, I, Kotin, RM, Derksen, TA *et al.* (2000). Recombinant adeno-associated virus type 2, 4, and 5 vectors: transduction of variant cell types and regions in the mammalian central nervous system. *Proc Natl Acad Sci U S A* **97**: 3428–3432.
4. Samaranch, L, Salegio, EA, San Sebastian, W, Kells, AP, Bringas, JR, Forsayeth, J *et al.* (2013). Strong cortical and spinal cord transduction after AAV7 and AAV9 delivery into the cerebrospinal fluid of nonhuman primates. *Hum Gene Ther* **24**: 526–532.
5. Merienne, N, Le Douce, J, Faivre, E, Déglon, N and Bonvento, G (2013). Efficient gene delivery and selective transduction of astrocytes in the mammalian brain using viral vectors. *Front Cell Neurosci* **7**: 106.
6. Dodiya, HB, Bjorklund, T, Stansell, J 3rd, Mandel, RJ, Kirik, D and Kordower, JH (2010). Differential transduction following basal ganglia administration of distinct pseudotyped AAV capsid serotypes in nonhuman primates. *Mol Ther* **18**: 579–587.
7. Taymans, JM, Vandenberghe, LH, Haute, CV, Thiry, I, Deroose, CM, Mortelmans, L *et al.* (2007). Comparative analysis of adeno-associated viral vector serotypes 1, 2, 5, 7, and 8 in mouse brain. *Hum Gene Ther* **18**: 195–206.
8. Sanchez, CE, Tierney, TS, Gale, JT, Alavian, KN, Sahin, A, Lee, JS *et al.* (2011). Recombinant adeno-associated virus type 2 pseudotypes: comparing safety, specificity, and transduction efficiency in the primate striatum. Laboratory investigation. *J Neurosurg* **114**: 672–680.
9. Zhang, HS, Kim, E, Lee, S, Ahn, IS and Jang, JH (2012). Transduction of striatum and cortex tissues by adeno-associated viral vectors produced by herpes simplex virus- and baculovirus-based methods. *J Virol Methods* **179**: 276–280.
10. Ciesielska, A, Hadaczek, P, Mittermeyer, G, Zhou, S, Wright, JF, Bankiewicz, KS *et al.* (2013). Cerebral infusion of AAV9 vector-encoding non-self proteins can elicit cell-mediated immune responses. *Mol Ther* **21**: 158–166.
11. Samaranch, L, San Sebastian, W, Kells, AP, Salegio, EA, Heller, G, Bringas, JR *et al.* (2014). AAV9-mediated expression of a non-self protein in nonhuman primate central nervous system triggers widespread neuroinflammation driven by antigen-presenting cell transduction. *Mol Ther* **22**: 329–337.
12. Harper, SQ, Staber, PD, He, X, Eliason, SL, Martins, IH, Mao, Q *et al.* (2005). RNA interference improves motor and neuropathological abnormalities in a Huntington's disease mouse model. *Proc Natl Acad Sci USA* **102**: 5820–5825.
13. McBride, JL, Boudreau, RL, Harper, SQ, Staber, PD, Monteys, AM, Martins, I *et al.* (2008). Artificial miRNAs mitigate shRNA-mediated toxicity in the brain: implications for the therapeutic development of RNAi. *Proc Natl Acad Sci USA* **105**: 5868–5873.
14. Franich, NR, Fitzsimons, HL, Fong, DM, Klugmann, M, During, MJ and Young, D (2008). AAV vector-mediated RNAi of mutant huntingtin expression is neuroprotective in a novel genetic rat model of Huntington's disease. *Mol Ther* **16**: 947–956.
15. Boudreau, RL, McBride, JL, Martins, I, Shen, S, Xing, Y, Carter, BJ *et al.* (2009). Nonallele-specific silencing of mutant and wild-type huntingtin demonstrates therapeutic efficacy in Huntington's disease mice. *Mol Ther* **17**: 1053–1063.
16. Stanek, LM, Sardi, SP, Mastis, B, Richards, AR, Treleaven, CM, Taksir, T *et al.* (2014). Silencing mutant huntingtin by adeno-associated virus-mediated RNA interference ameliorates disease manifestations in the YAC128 mouse model of Huntington's disease. *Hum Gene Ther* **25**: 461–474.

17. Han, I, You, Y, Kordower, JH, Brady, ST and Morfini, GA (2010). Differential vulnerability of neurons in Huntington's disease: the role of cell type-specific features. *J Neurochem* **113**: 1073–1091.
18. Vonsattel, JP (2008). Huntington disease models and human neuropathology: similarities and differences. *Acta Neuropathol* **115**: 55–69.
19. Wang, N, Gray, M, Lu, XH, Cantle, JP, Holley, SM, Greiner, E *et al.* (2014). Neuronal targets for reducing mutant huntingtin expression to ameliorate disease in a mouse model of Huntington's disease. *Nat Med* **20**: 536–541.
20. Foust, KD, Nurre, E, Montgomery, CL, Hernandez, A, Chan, CM and Kaspar, BK (2009). Intravascular AAV9 preferentially targets neonatal neurons and adult astrocytes. *Nat Biotechnol* **27**: 59–65.
21. Gray, SJ, Matagne, V, Bachaboina, L, Yadav, S, Ojeda, SR and Samulski, RJ (2011). Preclinical differences of intravascular AAV9 delivery to neurons and glia: a comparative study of adult mice and nonhuman primates. *Mol Ther* **19**: 1058–1069.
22. Dufour, BD, Smith, CA, Clark, RL, Walker, TR and McBride, JL (2014). Intrajugular vein delivery of AAV9-RNAi prevents neuropathological changes and weight loss in Huntington's disease mice. *Mol Ther* **22**: 797–810.
23. Richardson, RM, Kells, AP, Martin, AJ, Larson, PS, Starr, PA, Piferi, PG *et al.* (2011). Novel platform for MRI-guided convection-enhanced delivery of therapeutics: preclinical validation in nonhuman primate brain. *Stereotact Funct Neurosurg* **89**: 141–151.
24. Richardson, RM, Gimenez, F, Salegio, EA, Su, X, Bringas, J, Berger, MS *et al.* (2011). T2 imaging in monitoring of intraparenchymal real-time convection-enhanced delivery. *Neurosurgery* **69**: 154–63; discussion 163.
25. Richardson, RM, Kells, AP, Rosenbluth, KH, Salegio, EA, Fiandaca, MS, Larson, PS *et al.* (2011). Interventional MRI-guided putaminal delivery of AAV2-GDNF for a planned clinical trial in Parkinson's disease. *Mol Ther* **19**: 1048–1057.
26. Bankiewicz, KS, Eberling, JL, Kohutnicka, M, Jagust, W, Pivirotto, P, Bringas, J *et al.* (2000). Convection-enhanced delivery of AAV vector in parkinsonian monkeys; *in vivo* detection of gene expression and restoration of dopaminergic function using pro-drug approach. *Exp Neurol* **164**: 2–14.
27. Rosenbluth, KH, Luz, M, Mohr, E, Mittermeyer, S, Bringas, J and Bankiewicz, KS (2011). Design of an in-dwelling cannula for convection-enhanced delivery. *J Neurosci Methods* **196**: 118–123.
28. Aschauer, DF, Kreuz, S and Rumpel, S (2013). Analysis of transduction efficiency, tropism and axonal transport of AAV serotypes 1, 2, 5, 6, 8 and 9 in the mouse brain. *PLoS One* **8**: e76310.
29. Clark, KR, Liu, X, McGrath, JP and Johnson, PR (1999). Highly purified recombinant adeno-associated virus vectors are biologically active and free of detectable helper and wild-type viruses. *Hum Gene Ther* **10**: 1031–1039.
30. Burnham, B, Nass, S, Kong, E, Mattingly, M, Woodcock, D, Song, A *et al.* (2015). Analytical Ultracentrifugation as an Approach to Characterize Recombinant Adeno-Associated Viral Vectors. *Hum Gene Ther Methods* **26**: 228–242.
31. Bartus, RT, Kordower, JH, Johnson, EM Jr, Brown, L, Kruegel, BR, Chu, Y *et al.* (2015). Post-mortem assessment of the short and long-term effects of the trophic factor neurturin in patients with α-synucleinopathies. *Neurobiol Dis* **78**: 162–171.
32. McCown, TJ (2011). Adeno-Associated Virus (AAV) Vectors in the CNS. *Curr Gene Ther* **11**: 181–188.
33. Morton, AJ and Howland, DS (2013). Large genetic animal models of Huntington's Disease. *J Huntingtons Dis* **2**: 3–19.
34. Vonsattel, JP, Keller, C and Cortes Ramirez, EP (2011). Huntington's disease - neuropathology. *Handb Clin Neurol* **100**: 83–100.
35. Vonsattel, JP, Myers, RH, Stevens, TJ, Ferrante, RJ, Bird, ED and Richardson, EP Jr (1985). Neuropathological classification of Huntington's disease. *J Neuropathol Exp Neurol* **44**: 559–577.
36. Watakabe, A, Ohtsuka, M, Kinoshita, M, Takaji, M, Isa, K, Mizukami, H *et al.* (2015). Comparative analyses of adeno-associated viral vector serotypes 1, 2, 5, 8 and 9 in marmoset, mouse and macaque cerebral cortex. *Neurosci Res* **93**: 144–157.
37. Markakis, EA, Vives, KP, Bober, J, Leichtle, S, Leranth, C, Beecham, J *et al.* (2010). Comparative transduction efficiency of AAV vector serotypes 1-6 in the substantia nigra and striatum of the primate brain. *Mol Ther* **18**: 588–593.
38. Burger, C, Gorbatyuk, OS, Velardo, MJ, Peden, CS, Williams, P, Zolotukhin, S *et al.* (2004). Recombinant AAV viral vectors pseudotyped with viral capsids from serotypes 1, 2, and 5 display differential efficiency and cell tropism after delivery to different regions of the central nervous system. *Mol Ther* **10**: 302–317.
39. Hadaczek, P, Kohutnicka, M, Krauze, MT, Bringas, J, Pivirotto, P, Cunningham, J *et al.* (2006). Convection-enhanced delivery of adeno-associated virus type 2 (AAV2) into the striatum and transport of AAV2 within monkey brain. *Hum Gene Ther* **17**: 291–302.
40. Kaspar, BK, Erickson, D, Schaffer, D, Hinh, L, Gage, FH and Peterson, DA (2002). Targeted retrograde gene delivery for neuronal protection. *Mol Ther* **5**: 50–56.
41. Passini, MA, Macauley, SL, Huff, MR, Taksir, TV, Bu, J, Wu, IH *et al.* (2005). AAV vector-mediated correction of brain pathology in a mouse model of Niemann-Pick A disease. *Mol Ther* **11**: 754–762.
42. Kells, AP, Hadaczek, P, Yin, D, Bringas, J, Varenika, V, Forsayeth, J *et al.* (2009). Efficient gene therapy-based method for the delivery of therapeutics to primate cortex. *Proc Natl Acad Sci USA* **106**: 2407–2411.
43. Hollis, ER 2nd, Kadoya, K, Hirsch, M, Samulski, RJ and Tuszynski, MH (2008). Efficient retrograde neuronal transduction utilizing self-complementary AAV1. *Mol Ther* **16**: 296–301.
44. Castle, MJ, Gershenson, ZT, Giles, AR, Holzbaur, EL and Wolfe, JH (2014). Adeno-associated virus serotypes 1, 8, and 9 share conserved mechanisms for anterograde and retrograde axonal transport. *Hum Gene Ther* **25**: 705–720.
45. San Sebastian, W, Richardson, RM, Kells, AP, Lamarre, C, Bringas, J, Pivirotto, P *et al.* (2012). Safety and tolerability of magnetic resonance imaging-guided convection-enhanced delivery of AAV2-hAADC with a novel delivery platform in nonhuman primate striatum. *Hum Gene Ther* **23**: 210–217.
46. Hadaczek, P, Eberling, JL, Pivirotto, P, Bringas, J, Forsayeth, J and Bankiewicz, KS (2010). Eight years of clinical improvement in MPTP-lesioned primates after gene therapy with AAV2-hAADC. *Mol Ther* **18**: 1458–1461.
47. Wang, C, Wang, CM, Clark, KR and Sferra, TJ (2003). Recombinant AAV serotype 1 transduction efficiency and tropism in the murine brain. *Gene Ther* **10**: 1528–1534.
48. Yang, GS, Schmidt, M, Yan, Z, Lindbloom, JD, Harding, TC, Donahue, BA *et al.* (2002). Virus-mediated transduction of murine retina with adeno-associated virus: effects of viral capsid and genome size. *J Virol* **76**: 7651–7660.
49. Summerford, C and Samulski, RJ (1998). Membrane-associated heparan sulfate proteoglycan is a receptor for adeno-associated virus type 2 virions. *J Virol* **72**: 1438–1445.
50. Wu, Z, Miller, E, Agbandje-McKenna, M and Samulski, RJ (2006). Alpha2,3 and alpha2,6 N-linked sialic acids facilitate efficient binding and transduction by adeno-associated virus types 1 and 6. *J Virol* **80**: 9093–9103.
51. McBride, JL, Pitzer, MR, Boudreau, RL, Dufour, B, Hobbs, T, Ojeda, SR *et al.* (2011). Preclinical safety of RNAi-mediated HTT suppression in the rhesus macaque as a potential therapy for Huntington's disease. *Mol Ther* **19**: 2152–2162.
52. Parent, A and Hazrati, LN (1995). Functional anatomy of the basal ganglia. I. The cortico-basal ganglia-thalamo-cortical loop. *Brain Res Brain Res Rev* **20**: 91–127.
53. Haber, SN and Knutson, B (2010). The reward circuit: linking primate anatomy and human imaging. *Neuropsychopharmacology* **35**: 4–26.
54. McFarland, NR and Haber, SN (2002). Thalamic relay nuclei of the basal ganglia form both reciprocal and nonreciprocal cortical connections, linking multiple frontal cortical areas. *J Neurosci* **22**: 8117–8132.
55. Künzle, H (1975). Bilateral projections from precentral motor cortex to the putamen and other parts of the basal ganglia. An autoradiographic study in Macaca fascicularis. *Brain Res* **88**: 195–209.
56. Hadaczek, P, Yamashita, Y, Mirek, H, Tamas, L, Bohn, MC, Noble, C *et al.* (2006). The "perivascular pump" driven by arterial pulsation is a powerful mechanism for the distribution of therapeutic molecules within the brain. *Mol Ther* **14**: 69–78.
57. Forsayeth, J and Bankiewicz, KS (2015). Transduction of antigen-presenting cells in the brain by AAV9 warrants caution in preclinical studies. *Mol Ther* **23**: 612.
58. San Sebastian, W, Kells, AP, Bringas, J, Samaranch, L, Hadaczek, P, Ciesielska, A *et al.* (2014). Safety and tolerability of MRI-guided infusion of AAV2-hAADC into the mid-brain of non-human primate. *Mol Ther Methods Clin Dev* **3**: 14049.
59. San Sebastian, W, Samaranch, L, Heller, G, Kells, AP, Bringas, J, Pivirotto, P *et al.* (2013). Adeno-associated virus type 6 is retrogradely transported in the non-human primate brain. *Gene Ther* **20**: 1178–1183.
60. Xiao, X, Li, J and Samulski, RJ (1998). Production of high-titer recombinant adeno-associated virus vectors in the absence of helper adenovirus. *J Virol* **72**: 2224–2232.
61. Thorne, BA, Takeya, RK and Peluso, RW (2009). Manufacturing recombinant adeno-associated viral vectors from producer cell clones. *Hum Gene Ther* **20**: 707–714.
62. Martin, J, Frederick, A, Luo, Y, Jackson, R, Joubert, M, Sol, B *et al.* (2013). Generation and characterization of adeno-associated virus producer cell lines for research and preclinical vector production. *Hum Gene Ther Methods* **24**: 253–269.
63. Qu, G, Bahr-Davidson, J, Prado, J, Tai, A, Cataniag, F, McDonnell, J *et al.* (2007). Separation of adeno-associated virus type 2 empty particles from genome containing vectors by anion-exchange column chromatography. *J Virol Methods* **140**: 183–192.
64. Grimm, D, Kay, MA and Kleinschmidt, JA (2003). Helper virus-free, optically controllable, and two-plasmid-based production of adeno-associated virus vectors of serotypes 1 to 6. *Mol Ther* **7**: 839–850.

Supplementary Information accompanies this paper on the *Molecular Therapy—Methods & Clinical Development* website (http://www.nature.com/mtm)